Fluid Phase Equilibria 313 (2012) 16–24

Contents lists available at SciVerse ScienceDirect

Fluid Phase Equilibria

journal homepage: www.elsevier.com/locate/fluid

Molecular dynamics study of vapor–liquid equilibria and transport properties of sodium and lithium based on EAM potentials

Atanu K. Metya, Abhiram Hens, Jayant K. Singh*

Department of Chemical Engineering, Indian Institute of Technology Kanpur, Kanpur 208016, India

ARTICLE INFO

Article history:
Received 6 July 2011
Received in revised form 25 August 2011
Accepted 27 August 2011
Available online 29 September 2011

Keywords:
Sodium
Lithium
Vapor–liquid
Diffusivity
Shear viscosity
Scaling laws
EAM
Molecular dynamics

ABSTRACT

We present the equilibrium and dynamical properties of liquid sodium (Na) and lithium (Li), based on embedded atom models, using molecular dynamics simulations. In particular, we present vapor–liquid equilibria, critical properties, diffusivity, shear viscosity and excess entropy of liquid Na and Li. Critical temperatures obtained in the current work are 2462 K and 5649 K for Na and Li, respectively. On the other hand, critical density for Na is 0.3493 g/cm^3 and that for Li is 0.1553 g/cm^3. Critical pressures based on the exiting EAM models for Na and Li are 113 bar and 1686 bar, respectively. The relation of excess entropy and dynamical properties is examined in the framework of existing scaling laws. We observed an exponential nature between the dimensionless scaled diffusion constant and the approximate excess entropy for liquid Na and Li, as also observed for other liquid metals.

1. Introduction

Thermophysical properties such as the vapor–liquid equilibrium data of various metallic liquids are extremely useful in numerous technological applications. Starting from domestic clinical thermometer to high temperature nuclear reactor, from metallurgical industry to electronic industry, liquid metals are of significant usage [1–5]. Hence, these fluids are being studied by various means. Experiments with liquid metals are difficult to conduct due to the associated high temperature and pressure; consequently, theoretical and molecular simulations are widely popular means to study liquid metals.

Absence of suitable force fields for liquid metals was a big hindrance in the study of these materials for a long time. An effort was made using Morse potential and central force model to calculate the elastic constant of a few metals [6]. Although the results were satisfactory, the model had limitations. Quantum based band theory came into picture in the middle of the 20th century [7]. Cluster methods [8] also failed to handle the size effect. Next, two body interaction potentials or pair potential methods were derived both from fundamental considerations [9,10] and experimental means [11,12]. From this pair potential method, the energy calculation was direct; however, it required the use of volume dependent energy to describe the elastic properties of the metal. Exact calculation of this volume is often difficult in certain systems like ones with surfaces, fractures, etc. Moreover this pair potential method was not applicable in the case of chemically active species. In order to include all surfaces, fractures, impurities, alloys, etc., Daw and Baskes proposed the concept of embedded atom method in 1983 [13,14]. The embedded atom method was applied for few liquid transition metals and the results were in good agreement with the experimental data which supported the applicability of the EAM method [15,16].

Molecular simulation study of liquid Na was started about 30 years back with molecular dynamics study of liquid Na near its melting point by Miranda and Torra [17]. Using five different potential functions computed from a local pseudopotential and a variety of dielectric functions, some properties like specific heat and radial distribution functions were calculated. Maiti and Falicov [18] derived a phase diagram for Na clusters up to $N = 1000$ based on first order pseudopotential calculations and the Lindeman criterion for melting. Some experimental works on melting of dense Na at different pressures were done by Gregoryanz et al. [19]. The Morse potential energy function was formulated for describing pair potential functions for metals [20,21]. Lincoln et al. [6] further refined the Morse potential for different metals using some experimental data. Using these potentials vapor–liquid coexistence curves were studied for different metals including Na by Singh et al. [22]. On the other hand, very few works on the vapor–liquid

* Corresponding author. Tel.: +91 512 2596141; fax: +91 512 2590104.
E-mail addresses: atanumta@iitk.ac.in (A.K. Metya), hens.abhiram@gmail.com (A. Hens), jayantks@iitk.ac.in (J.K. Singh).

0378-3812/$ – see front matter © 2011 Elsevier B.V. All rights reserved.
doi:10.1016/j.fluid.2011.08.026

phase equilibria of metals are reported using more precise models such as EAM. For example, Bhatt et al. [23] have calculated critical properties of aluminium using EAM potentials and Aleksandrov et al. [24] calculated VLE data of Cu using EAM potential. Similar to the case of liquid sodium, not much work has been done to obtain vapor–liquid coexistence of other alkali metals such as Li. Though, using molecular dynamics some work on liquid lithium based on inter ionic effective potential has been reported by Canales et al. [25,26] and the results were in good agreement with experiments [26–28].

One of the objectives, in this work, is to investigate the VLE of alkali metals, in particular of sodium and lithium based on newly formulated EAM models [29,30]. In addition to the phase equilibria, we also investigate the structure–dynamical property relations, in the context of entropy scaling law, of these liquid metals. The idea of entropy scaling law relationship for transport coefficients started around 1977 for simple liquids. The excess entropy is important in the case of monatomic liquids since many transport properties such as diffusivity and viscosity follow the scaling relationship [31–34]. The excess entropy is defined as the difference between the liquid and that of the equivalent ideal gas. The excess entropy can be approximated by the two body approximation [35,36] which is denoted by S_2 and is given by

$$S_2 = -2\pi\rho \int \{g(r)\ \ln[g(r)] - [g(r) - 1]\} r^2\, dr, \tag{1}$$

where $g(r)$ is the radial distribution function (RDF), ρ is the number density, and S_2 is given in unit of k_B per particle. The advantage of using RDF is that this quantity is readily measurable in either experiments or simulations. S_2, though approximate measure, can provide an accurate structural measure of the thermodynamics excess entropy. Using EAM models [16,37,38], various workers have studied structural and transport properties of liquid metals, and its scaling law relating the structural and dynamical properties [39]. However, scaling law analysis of structure–dynamics relation has not been studied well for alkali metals using EAM models.

Dzugutov [40] proposed a universal scaling law, which relates the diffusion coefficient to excess entropy (S_2). The scaled diffusion coefficient, $D^* = D/\sigma^2\Gamma$, for simple liquids system, is related to the excess entropy through the following relation

$$D^* = \frac{D}{\sigma^2\Gamma} = 0.049\ \ \exp(S_2), \tag{2}$$

where D is the self diffusivity, σ is the hard sphere diameter and Γ is the collision frequency which according to Enskog theory [41] is:

$$\Gamma = 4\sigma^2 g(\sigma)\rho\sqrt{\frac{\pi k_B T}{m}}, \tag{3}$$

where $g(\sigma)$ is the RDF evaluated at the hard sphere diameter, ρ is the number density, T is the absolute temperature, k_B is the Boltzmann constant and m is the atomic mass. The above scaling law was reconfirmed by Hoyt et al. [39] using a computer simulation using EAM models for some liquid metals. They observed some scatter in the data; however, with the use of the more accurate excess entropy calculation rather than the S_2 form, there appears to be less scatter in the data.

In another approach, microscopic reduction parameters (density and temperature) were chosen for the transport coefficients, viz. a mean interparticle distance, $d = (V/N)^{1/3} = \rho^{1/3}$, and the velocity, $v_{th} = (k_B T/m)^{1/2}$. Rosenfeld [32,34] defines the following dimensionless scaled diffusion coefficient:

$$D^* = D\frac{\rho^{1/3}}{(k_B T/m)^{1/2}}. \tag{4}$$

Based on hundreds of simulation results for the dimensionless scaled diffusion coefficient, Rosenfeld [32,34] proposed the scaling law as

$$D^* = A\ \ \exp(\alpha S_2), \tag{5}$$

with A equal to 0.6 and α equal to 0.8. This semi-empirical scaling law was recognized by many authors [42–44].

The second objective of this work is to calculate dynamical properties viz., diffusivity and shear viscosity, of the liquid alkaline metals, Na and Li, using EAM potential proposed by Belashchenko [29,30] and examine the relationship between excess entropy and scaled diffusivity.

The paper is organized as follows. In the next section, we present the force field used to model the interactions between atoms. Section 3 introduces the methodology and simulation details. Section 4 presents the simulation results and that is followed by the conclusions.

2. Model

The embedded atom model, or EAM, describing the energy between two atoms and is related to the second moment approximation to tight binding theory. These models are particularly appropriate for metallic systems. The original model was proposed by Daw and Baskes [13]. The potential energy of a monoatomic system is represented as [29,30]

$$U_{pot} = \sum_i \Phi(\rho_i) + \sum_{i<j} \varphi(r_{ij}), \tag{6}$$

where $\Phi(\rho_i)$ is the embedding potential of the ith atom which depends on the effective electron density $\rho_i = \sum_j \psi(r_{ij})$, at the point of location of the centre of the atom, $\psi(r_{ij})$ is the contribution to electron density and j represents the neighbor atoms. $\varphi(r_{ij})$ is simple pair potential between ith and jth atom. r_{ij} is the distance between ith and jth atom.

The function $\Phi(\rho_i)$ for liquid sodium [29] is parameterized as

$$\Phi(\rho) = a_1 + c_1(\rho - \rho_0)^2 \quad \text{at} \quad \rho_1 < \rho < \rho_6, \tag{7}$$

$$\Phi(\rho) = a_i + b_i(\rho - \rho_{i-1})(\rho - \rho_{i-1}) + c_i(\rho - \rho_{i-1})^2 \quad \text{at} \quad \rho_i < \rho < \rho_{i-1} \quad (i = 2, 3, 4, 5), \tag{8}$$

$$\Phi(\rho) = [a_6 + b_6(\rho - \rho_5) + c_6(\rho - \rho_5)^2]\left[2\frac{\rho}{\rho_5} - \left(\frac{\rho}{\rho_5}\right)^2\right] \quad \text{at} \quad \rho < \rho_5, \tag{9}$$

$$\Phi(\rho) = a_7 + b_7(\rho - \rho_6) + c_7(\rho - \rho_6)^m \quad \text{at} \quad \rho_6 < \rho < \rho_7, \tag{10}$$

$$\Phi(\rho) = a_8 + b_8(\rho - \rho_7) + c_8(\rho - \rho_7)^n \quad \text{at} \quad \rho > \rho_7. \tag{11}$$

In case of lithium, the expression of embedding potential is not much different. Eqs. (7) and (8) are used in addition to the following equations for the case of lithium [30]:

$$\Phi(\rho) = [a_6 + b_6(\rho - \rho_1) + c_6(\rho - \rho_1)^2]\left[2\frac{\rho}{\rho_5} - \left(\frac{\rho}{\rho_5}\right)^2\right] \quad \text{at} \quad \rho < \rho_5, \tag{12}$$

$$\Phi(\rho) = a_7 + b_7(\rho - \rho_0)^m \quad \text{at} \quad \rho \geq \rho_6. \tag{13}$$

Table 1
Parameters of embedding functions and electron density for liquid sodium [29] and lithium [30].

	Parameters								
	ρ_{0-7}	a_i	b_i	c_i	m	n	p_1	p_2	r_c (Å)
Na	1.0000	−0.33140		0.1619	1.15	1.42	3.4418	1.0245	10.78
	0.9000	−0.32980	−0.3238	−0.170					
	0.8000	−0.32820	0.00162	−0.275					
	0.7000	−0.3312	0.05662	0.600					
	0.6200	−0.3318	0.15262	0.880					
	0.2800	−0.282	−0.4458	5.000					
	1.1700	−0.3267	0.05505	−0.100					
	2.6000	−0.3989	−0.0663	0.3350					
Li	1.0000	−0.880900		0.0430	1.50		3.04500	1.22000	7.50
	0.9000	−0.880470	−0.008600	2.000000					
	0.8400	−0.872754	−0.248400	−1.09000					
	0.7000	−0.859314	0.0566000	1.300000					
	0.4800	−0.808846	−0.515400	0.300000					
	0.4200	−0.776842	−0.551400	0.000000					
	1.1000	−0.881043	0.0181304						

The electron density function is taken in the form [29,30]

$$\psi(r) = p_1 \exp(-p_2 r). \tag{14}$$

The pair potential for liquid sodium [29] is defined in the following form

$$\varphi(r) = 0.786149 \exp[1.2(2.55 - r)]\,(\text{eV}) \quad \text{at} \quad r \le 2.25\,\text{Å}, \tag{15}$$

$$\varphi_m(r) = b_{m0} + \sum_{n=1}^{6} b_{mn}(r - r_m)^n$$

$$\text{at} \quad r_{m-1} < r < r_m \quad (m = 2, \ldots, 11). \tag{16}$$

In case of liquid lithium, the pair potential form is [30]:

$$\varphi(r) = 0.401569 \exp[2.10(2.35 - r)]\,(\text{eV}) \quad \text{at} \quad r \le 2.35\,\text{Å}. \tag{17}$$

Tables 1 and 2 summarize all the parameters of the potentials for liquid sodium and lithium.

3. Methodology and simulation detail

3.1. Analysis of vapor–liquid phase transition

In this work, the interfacial thickness calculated from the fit of the density profile obtained from NVT simulations to the following expression [45].

$$\rho(z) = 0.5(\rho_l + \rho_v) - 0.5(\rho_l - \rho_v) erf\left(\frac{\sqrt{\pi}(z - l)}{d}\right), \tag{18}$$

where ρ_l and ρ_v are coexisting densities of liquid and vapor phases, respectively; d is the interfacial width; and l is the position for Gibbs dividing surface.

The critical parameters are estimated by using the coexistence data (obtained from fitting profiles for various sub critical temperatures) and the least squares fit of the following scaling law [46]:

$$\rho_l - \rho_v = C_1\left(1 - \frac{T}{T_c}\right)^{\beta_c}, \tag{19}$$

where ρ_l and ρ_v are coexisting densities of liquid and vapor phases, respectively, and C_1 and β_c are fitting parameters. The critical temperature T_c obtained from the above equation is used to calculate the critical density, ρ_c, from the least square fit to the law of rectilinear diameter [47]:

$$\frac{(\rho_l + \rho_v)}{2} = \rho_c + C_2(T - T_c), \tag{20}$$

where C_2 is the fitting parameter.

Critical pressure is evaluated using the least square fitting to the following expression:

$$\ln\ P = A + \frac{B}{T}, \tag{21}$$

where A and B are constants.

3.2. Diffusivity and shear viscosity calculations

The diffusion coefficient (D) can be obtained using two equivalent equilibrium methods [48]. One is the Einstein relation, where diffusion coefficient is related to the slope of the mean square displacement (MSD) of the particles over time:

$$D = \frac{1}{6}\lim_{t\to\infty} \frac{d}{dt}\left\langle [r_i(t + t_0) - r_i(t_0)]^2 \right\rangle. \tag{22}$$

Another one is the Green–Kubo (GK) integration over the velocity autocorrelation function

$$D = \frac{1}{3}\int_0^\infty V_i(t + t_0) \cdot V_0(t_0)\, dt. \tag{23}$$

The shear viscosity can be determined using GK integration over autocorrelation function (ACF) of $P_{\alpha\beta}$, the off diagonal pressure tensor components

$$\eta = \frac{V}{k_B T}\int_0^\infty \left\langle P_{\alpha\beta}(t + t_0) \cdot P_{\alpha\beta}(t_0)\right\rangle dt. \tag{24}$$

Phase equilibria of liquid sodium and lithium are evaluated using the slab based molecular simulation technique [49,50]. In particular, molecular dynamics in the canonical (NVT) ensemble using LAMMPS [51] is conducted, and the vapor–liquid density profile of the coexisting vapor and liquid phases is used to obtain the coexistence saturated densities. In this work, we have considered N = 8000 atoms for Na and N = 16,000 atoms for Li. Periodic boundary condition is applied in all the three directions. We start with the construction of the simulation box (see Fig. 1) with the liquid slab in the centre of a rectangular box. The length of the box along z direction is kept three times greater than those of x and y directions. The liquid slab in the box is in coexistence with the vapor phase filling

Table 2
Coefficients of pair potential in power of $(r - r_m)$ for sodium [29].

No. of interval (m)	Interval of distances $(r_{m-1} - r_m)$ (Å)	Coefficients series expansion							
		b_{m0}	b_{m1}	b_{m2}	b_{m3}	b_{m4}	b_{m5}	b_{m6}
2	2.55–2.80	0.35805506	−2.8231320	12.574037	324.38852	1675.1389	2599.4679	–
3	2.80–2.95	0.12708218	−0.78856218	1.4613397	−23.646932	–	–	–
4	2.95–3.45	−0.11093583	−0.30139562	−0.57444694	−7.6710592	−29.513198	−53.353203	−35.242442
5	3.45–3.95	−0.18380286	−0.031204076	0.66662912	4.8636249	20.310489	37.538781	25.743498
6	3.95–4.45	−0.17446597	0.094991311	0.61158912	3.8291921	12.551371	18.518679	10.122143
7	4.45–4.95	−0.13020295	0.087927282	−0.56735449	−5.2796190	−19.751878	−33.862967	−21.896864
8	4.95–5.45	−0.073686510	0.13220064	0.75321670	6.8207026	26.093839	45.498140	29.748444
9	5.45–5.95	−0.026368676	0.079378478	−0.076503428	−0.64246319	−3.6612803	−8.7641368	−7.2870333
10	5.95–7.45	0.028540069	−0.0019879458	0.005690421	0.080223638	0.099188093	0.06169853	0.014612381
11	7.45–10.78	0.73629497E−04	–	−0.40257317E−02	−0.52993510E−02	−0.16744300E−02	−0.42268470E−03	−0.65802071E−04

Fig. 1. Initial configuration for the vapor–liquid coexistence studies in the slab based method.

up rest of the simulation cell. There are two vapor–liquid interfaces in the simulation box due to the periodic boundary condition applied. A time step of 0.5 fs is fixed for both Na and Li. For Na 10^6 time steps are provided for equilibration and another 6×10^{-5} time steps are taken for production. In case of Li, 1.8×10^6 and 1.2×10^6 time steps are taken for equilibration and production respectively. Nose–Hoover thermostat is considered for fixing the temperature in both the cases. For Na, slab based MD simulations are performed for temperature ranging from 400 K to 2000 K; and, for Li, the temperature range was 2000–5100 K. During the production step, we collect configurations for property evaluations. Using 600 configurations, we evaluate the average density profiles of liquid–vapor system. Similarly, we obtain the density profiles for different temperatures in both the cases. To simulate the diffusivity and shear viscosity of these alkaline metals, the canonical (NVT) ensemble based MD simulations are performed. The diffusion coefficient is calculated from MSD using Einstein formula Eq. (22), and shear viscosity is calculated using GK formalism Eq. (24).

4. Results and discussion

4.1. Vapor–liquid transition and interfacial properties

We start the discussion with Fig. 2, which shows the configurations with increasing temperature for sodium and lithium. An interesting observation seen in case of vapor phase of sodium is that with increase in the vapor density, atoms in the vapor phase aggregate. The aggregation is found to increase with temperature. This behavior is well known for metallic system [52]. Magnetic susceptibility and optical absorption measurements for alkali metals in the vapor phase also show a high concentration of clusters as the vapor density increases [52]. Metallic clusters in the vapor phase have substantially lower ionization energies and higher electron affinities compared to that of a single atom, as seen for cesium in the vapor phase [53]. Therefore the probability of electron transfer from one atom to a large cluster is effectively increases. The formation of high amount of diamagnetic aggregates in the critical region of fluid alkali metals is completely consistent with the behavior of the magnetic properties [54]. This behavior is not so apparent in case of lithium, though, in our simulations.

Fig. 3(a) and (b) presents the z directional density profiles of Na and Li at different temperatures, respectively. As the temperature increases, liquid density gradually decreases and the corresponding vapor density increases. However at lower temperature, we observe interesting accumulation of particle at the interface. This is evident for sodium closer to melting temperature. This behavior is not seen in simple or dielectric fluids. The peaks at the interface in the low temperature density profiles are common in case of liquid metals. Density profile of liquid gallium also exhibits similar kind of peaks at the interface [55]. This may be due to the different nature of the force of interaction between the atoms in the two cases. The atomic interaction in liquid metal strongly depends on associated delocalized electron distribution; whereas in case of dielectric liquid, it depends on localized electron density only. As a result,

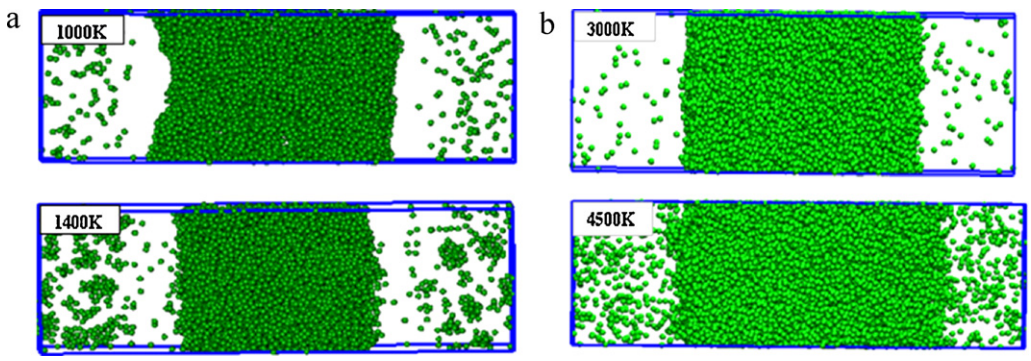

Fig. 2. Final configurations of the simulation box at different temperatures: (a) sodium and (b) lithium.

atomic interaction in liquid metal depends on the position of the inhomogeneous interface and the extent of this inhomogeneous transition zone is of the order of a few atomic diameters [55]. In case of a dielectric liquid, at temperatures near freezing point, the normal density distribution (along the z direction) falls monotonically from bulk liquid to bulk vapor value within two atomic diameter distances. This prediction is supported by experiments [56,57]. On the other hand for liquid metals, the longitudinal density distribution in the liquid–vapor interface, near the freezing point is predicted to have strong oscillations penetrating three to four atomic diameters into the bulk liquid [57–59]. We expect similar behavior for lithium at lower temperatures. Interfacial thicknesses obtained from fitting procedure [45] at different temperatures are shown in Fig. 4. The figure clearly illustrates the increase in the interfacial thicknesses with increasing temperature, as expected. Such behavior is akin to that seen for simple systems.

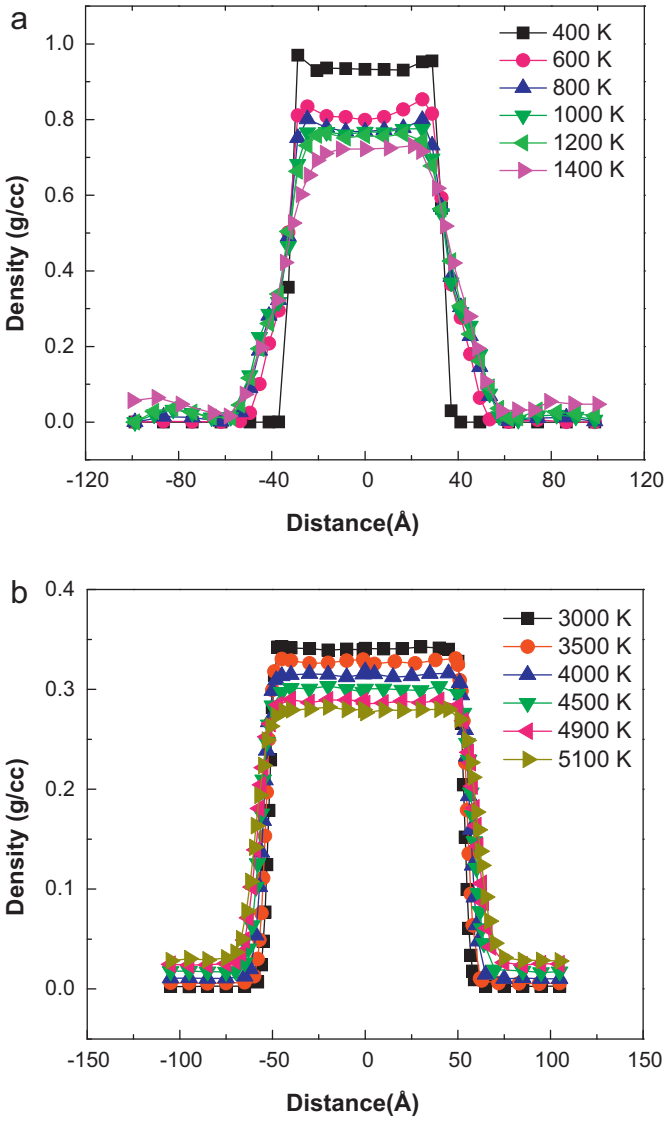

Fig. 3. Interfacial density profiles at different temperatures: (a) sodium and (b) lithium.

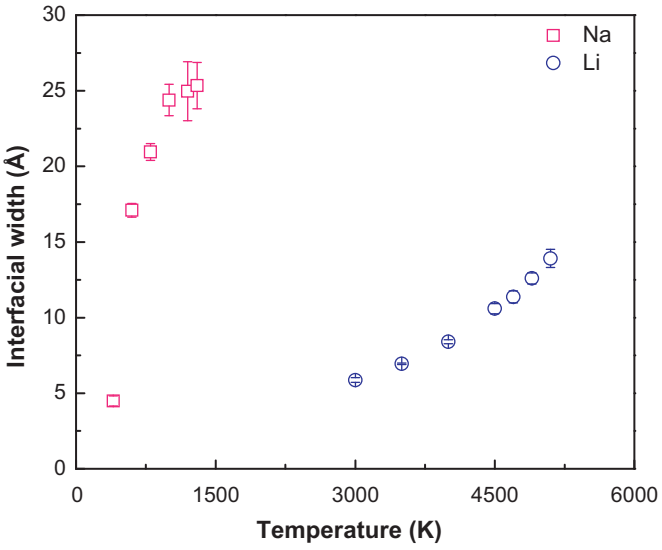

Fig. 4. Interfacial thickness as a function of temperature of sodium and lithium.

Fig. 5 presents the vapor–liquid coexistence data obtained from averaging $p(z)$ over appropriate regions. The vapor density is obtained by averaging the density profiles on both sides of the liquid film. The statistical error in the average densities is calculated from the standard deviation of block average densities. From the simulation results at different temperatures, critical temperature is determined using Eq. (19). Critical temperature for Na in this work is found to be 2462 K whereas experimental critical temperature is 2485 K [52]. Hence deviation from the experimental value is within 1%. Using this critical temperature, critical density, ρ_c was calculated using Eq. (20) and it is found to be 349.3 kg/m^3, which is about 16% higher than that known from the experiment, 300 kg/m^3 [52]. Results of critical temperature and density for Na, using Morse potential, by earlier workers [22], were 3932 K (T_c) and 353 kg/m^3 (ρ_c) respectively. Hence prediction of critical temperature and critical density using EAM potential is significantly better.

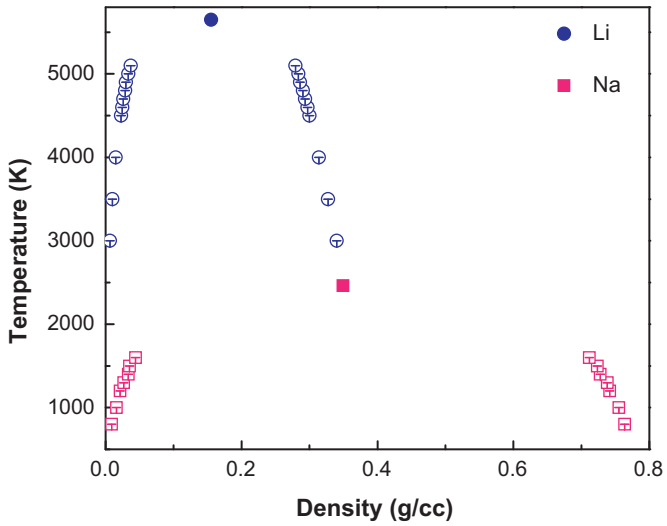

Fig. 5. Vapor–liquid coexistence curve for Na and Li. Error bars are within the symbol size.

In case of Li, following the same method mentioned above, critical temperature and critical density are calculated and found to be 5649 K and 0.1553 g/cm^3, respectively. There are no exact measurements of critical points for Li [60]. Estimates of critical temperatures vary well over 1000 K. However, Martynyuk [61] reported the values of critical temperature and density of Li as 3350 K and 0.086 gm/cm^3 respectively. The present results based on the EAM model of Li are over estimated with respect to Martynyuk data [61].

The vapor pressures for both the metals as a function of temperature are also estimated in this work. A separate molecular dynamics at a given vapor density under NVT ensemble is conducted to find the vapor pressure of the system. The vapor density is taken from the VLE data generated using slab based molecular dynamics method. Fig. 6 shows the plot of logarithmic vapor pressure as a function of inverse of temperature. The vapor pressure exhibits linear relationship below critical temperature in a semi-log scale against inverse of temperature. Hence, the Clausius–Clapeyron expression given by Eq. (21) is applicable and is used to determine the critical pressure for Na and Li metals. The estimated critical pressure of Na is 113 bar, which is lower than

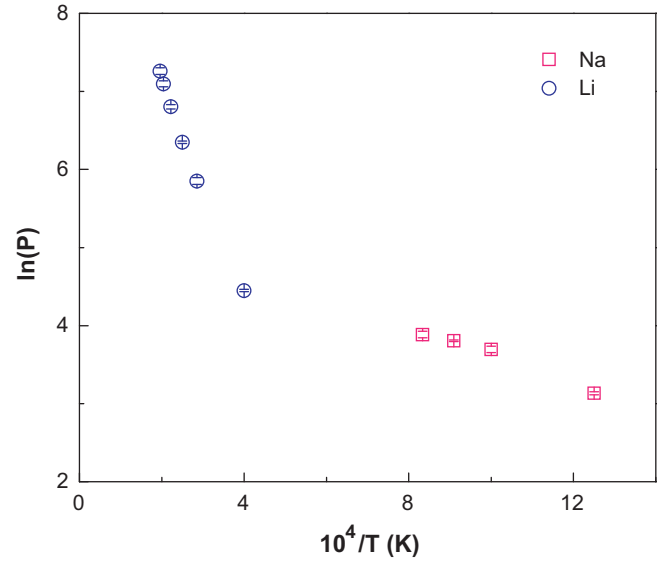

Fig. 6. Plot of saturation vapor pressure as function of inverse of temperature.

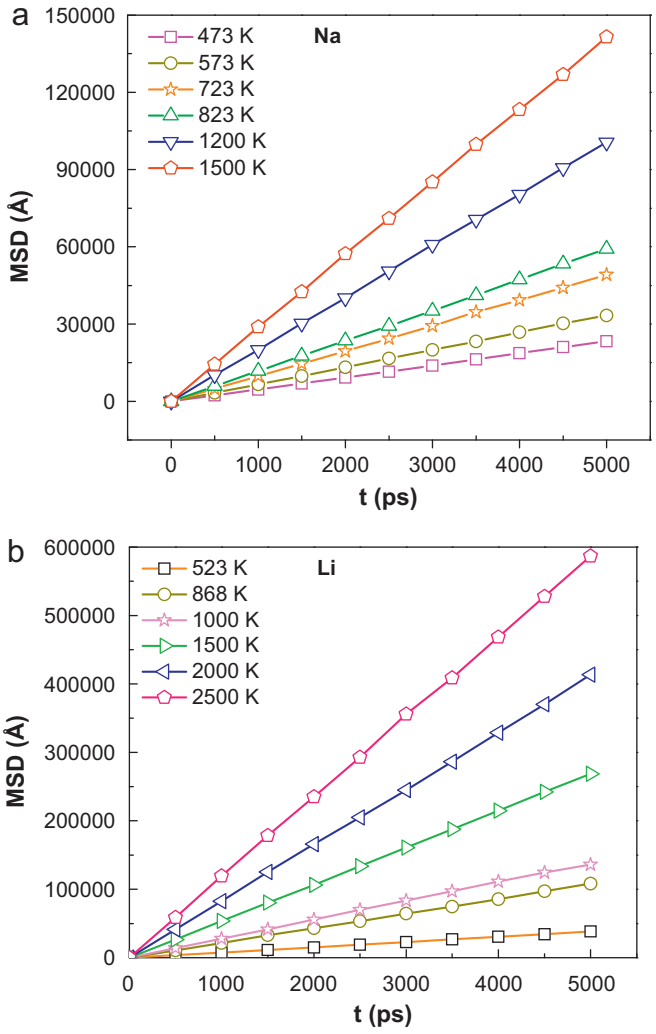

Fig. 7. The mean square displacements with time over a wide range of temperatures for liquid metals of (a) Na and (b) Li.

the available experimental value of 248 bar [52]. The Li critical pressure of 1686 bar is significantly higher than the reported value of 544 bar [61]. This critical pressure of Li is vastly over estimated due to larger critical temperature value estimated in this work.

4.2. Time-dependent transport coefficients and scaling law relationship

Fig. 7 displays the mean square displacement (MSD) of liquid Na and Li as a function of simulation time. The NVT simulations are conducted at saturated liquid conditions (densities) as obtained from the slab based molecular dynamic simulations. The slope of the curves in Fig. 7 is used to calculate self diffusivity according to Eq. (22). The shear viscosities (η) are computed by obtaining the pressure autocorrelation functions (PACF) for the off-diagonal components of pressure tensor by averaging over different time origins (see Eq. (24)). Fig. 8 presents the normalized values of the PACF for liquid Na and Li. It is interesting to note that the fluctuation in PACF decays very fast and, for both the cases, is quite small after ~1 ps and fluctuates around zero. This type of PACF is well known for liquid system like water [62]. In case of polymer system, the ACFs for the off-diagonal components of the pressure tensor in the short-time region differ from that in long time region [63]. Fig. 9 shows the shear viscosity as a function of integration time for Na

Table 3
Diffusivities (D) and shear viscosities (η) of liquid sodium and lithium at different temperatures.

	T (K)	Density (g/cm^3)	D (10^{-5} cm^2 s)			η (mPa s)		
			Our calc.	Expt.	Other MD	Our calc.	Expt.	Other MD
	378	0.3314	4.65 ± 0.07	4.32[a]				
	473	0.3240	7.79 ± 0.17	8.41[a]		0.380 ± 0.0131	0.450[f]	
	573	0.3202	11.18 ± 0.202	13[a]		0.292 ± 0.048	0.340[f]	
	673						0.278[f]	
	723	0.3061	16.411 ± 0.41			0.2412 ± 0.005		
Na	773						0.293[f]	
	823	0.2993	19.73 ± 0.455			0.2213 ± 0.002		
	873						0.212[f]	
	1200	0.2750	33.55 ± 0.462			0.1767 ± 0.004		
	1203						0.164[f]	
	1500	0.2556	47.16 ± 0.709			0.1465 ± 0.002		
	463	0.5139	9.99 ± 0.05	7.34[b]				
	470	0.5129	9.94 ± 0.24	6.4[c]	6.6, 6.3[c]	0.358 ± 0.009	0.57[e]	0.55[c]
	523	0.5090	12.76 ± 0.22			0.303 ± 0.002		
	843	0.4796	33.75 ± 0.54	25.8[d]	24.7, 25[c]	0.171 ± 0.004	0.30[d]	0.24[c]
Li	868	0.4777	35.85 ± 1.27			0.172 ± 0.005		
	1000	0.4639	45.88 ± 1.23			0.147 ± 0.001		
	1500	0.4139	88.33 ± 1.57			0.113 ± 0.004		
	2000	0.3679	136.23 ± 3.9			0.092 ± 0.003		
	2500	0.3242	196.83 ± 2.6					

[a] Ref. [64].
[b] Ref. [30].
[c] Ref. [26].
[d] Ref. [27].
[e] Refs. [27,28].
[f] Ref. [65]

and Li under the same conditions as for Fig. 8. Clearly, the shear viscosity is seen to converge convincingly.

There are a few experimental data of self diffusion and shear viscosity available for alkali metals. Table 3 lists both available simulation [26] and experimental data [26–28,30,64]. Fig. 10 shows MD results of diffusion coefficients, based on EAM potential, of liquid sodium and lithium at different temperatures along with available literature data. The nonlinear increase of the diffusivity with temperature is reliable; due to the collision frequency between atoms accelerates with increasing temperature. The comparison with experimental value shows that for liquid Na, the calculated results are close to the experimental data. However, in case of liquid Li, the present computed diffusion coefficient at 463 K is 10% larger than the experimental data [30]. In comparison to the MD results available in the literature for liquid lithium [26], the current EAM model for Lithium is incapable to capture the dynamical properties quantitatively. Fig. 11 shows the shear viscosity results of our present simulations for various temperatures compared with experimental data [26,27,65]. Fewer experimental results of shear viscosity are available for both the alkali metals. The present computed shear viscosity values of sodium reasonably agree with experimental data [65] at higher temperatures (above 700 K); however discrepancies are observed at lower temperatures. The calculated shear viscosity values of liquid lithium, using the EAM model, are considerably much lower compared to the available experimental values [26,27]. As observed for diffusivity results, the EAM model of lithium is inferior to the effective interaction available in the literatures [26,27,30].

Fig. 12(a) and (b) shows Dzugutov scaled diffusion coefficient D^*_{DZ} (Eq. (2)) and Rosenfeld scaled diffusion coefficient D^*_{RO} (Eq.

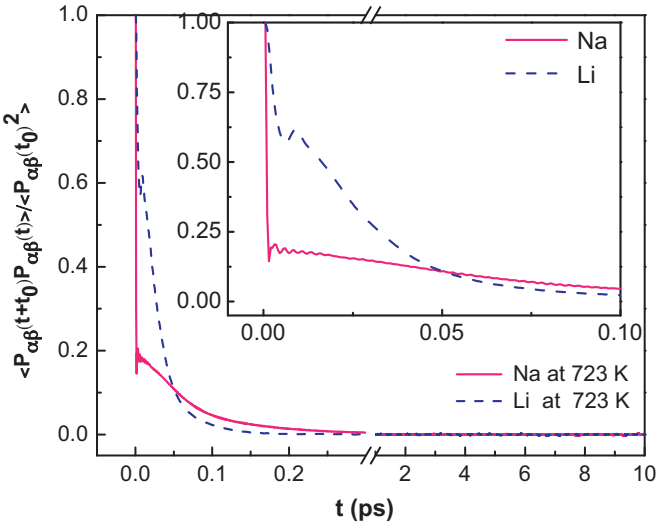

Fig. 8. Normalized autocorrelation functions of off-diagonal components of the pressure tensors. In the insert, an enlarged view of the short region is presented. The PACFs are averaged for 5 ns.

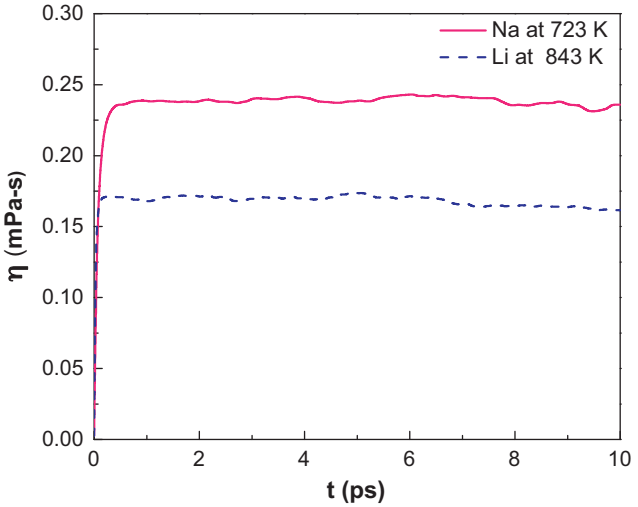

Fig. 9. The shear viscosity as a function of integration time.

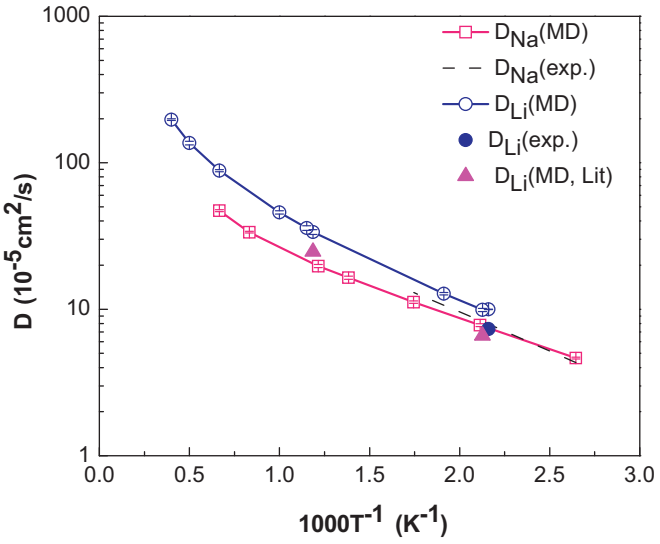

Fig. 10. Diffusion coefficient of liquid metals as a function of temperature. MD-Lit results of lithium are from Ref. [26].

(4)), versus two body approximation of excess entropy, S_2, as computed from Eq. (1). In Fig. 12(a) we compared the present simulation results to the original best fit determined by Dzugutov; this scaling law holds reasonably well for the pure liquid metals. Fig. 12(b) shows our simulation data are lower than the original work of Rosenfeld. The scattering of data in Fig. 12(a) and (b), does not mean an invalidity of the basic proposition of both the scaling laws, but it may suggest that the two body approximation of excess entropy S_2 is not completely reliable when utilizing many body EAM potentials. Hoyt et al. [39] also observed some scattering in the data from the Dzugutov scaling law for liquid transition metals using EAM potential. However, use of the more accurate calculation of excess entropy rather than the approximate S_2 form exhibits less scattering in the data. Baranyai and Evans [36] found that the difference between the actual excess entropy and the approximate S_2 value was nearly constant over a wide range of densities for Lennard–Jones system. However, based on our simulation results,

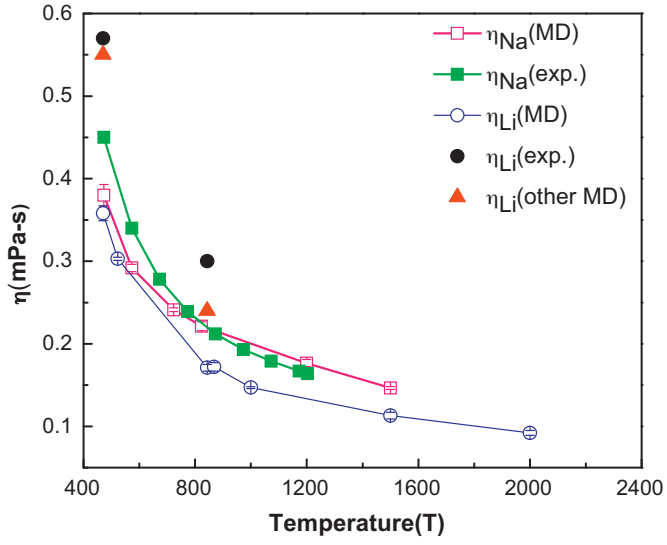

Fig. 11. Temperature dependence of the shear viscosity of liquid metals. Experimental data for Na are taken from Ref. [65]. MD-Lit results of lithium are from Ref. [26].

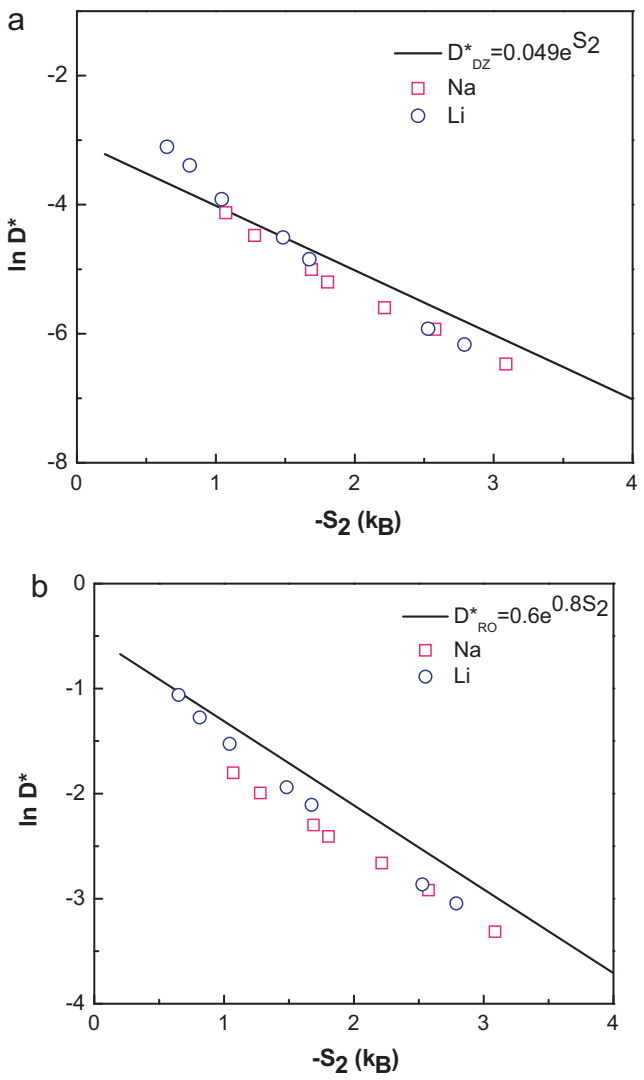

Fig. 12. The scaled diffusion coefficient versus the S_2, approximation of the excess entropy. The solid line is the scaling law of (a) Dzugutov (Eq. (2)) and (b) Rosenfeld (Eq. (5)).

we conclude that Dzugutov scaling law is more appropriate for alkali metals such as Na and Li.

5. Conclusion

We applied EAM potential to study the vapor–liquid phase transition, the structural and transport properties of liquid sodium and lithium from molecular dynamics using LAMMPS. Using slab based technique, we have calculated the vapor–liquid density profile and subsequently VLE of sodium and lithium using EAM model for the first time. Sodium atoms are found to accumulate near the interface at lower temperature similar to some other liquid metals. Finally, we have calculated the vapor–liquid phase diagram and found the critical temperature and density. For Na, the obtained critical temperature, 2462 K, is in good agreement with the experimental value, 2485 K. However, critical density estimate, in this case, is higher than the experimental work. In case of Li, the obtained values of critical temperature and density are 5649 K and 0.1553 g/cm^3, respectively, which are over estimated than the earlier reported results. We have also calculated the interfacial thickness of Na and Li at different temperatures and shear viscosity, diffusivity, and their variation with temperature and excess entropy. The calculated

diffusion coefficients of liquid sodium are in good agreement with experimental results. The shear viscosity of liquid sodium at higher temperature around 823 K is found to be 0.2213 mPa s. The results are in good agreement at higher temperatures but deviates from the experimental data at lower temperatures. The diffusivity and shear viscosity of liquid lithium are significantly higher and lower, respectively, compared to the experiments values. We also presented the reduced diffusion coefficient defined by Rosenfeld and excess entropy based on pair correlation function. Our results suggest that, both scaling laws are valid for alkali metals system. The above results clearly suggest that EAM model of liquid Na is reasonably robust; however, such is not the case for EAM model of liquid Li.

Acknowledgements

We would like to thank T.K. Patra and Dr. R. Srivastava for helpful discussions and suggestions. We specially thank Prof. D.K. Belashchenko for providing the EAM data. This work was supported by Indira Gandhi Centre for Atomic Research (IGCAR), Govt. of India.

Appendix A. Supplementary data

Supplementary data associated with this article can be found, in the online version, at doi:10.1016/j.fluid.2011.08.026.

References

[1] A.M. El-Kazzaz, A.C. Rose-Innes, J. Phys. D 20 (1987) 1616–1622.
[2] J.C. Poggendorff, Geschichte der Physik, Zentral-Antiquariat der DDR, Berlin, 1964.
[3] A.M. Nebrenchin, J. Min. Sci. 10 (1974) 623–625.
[4] Z. Djuric, P. Grant, Model. Simul. Mater. Sci. Eng. 9 (2001) 111–127.
[5] M.A. Jaworski, T.K. Gray, M. Antonelli, J.J. Kim, C.Y. Lau, M.B. Lee, M.J. Neumann, W. Xu, D.N. Ruzic, Phys. Rev. Lett. 104 (2010) 094503.
[6] R.C. Lincoln, K.M. Koliwad, P.B. Ghate, Phys. Rev. 157 (1967) 463–466.
[7] J.C. Slater, Quantum Theory of Matter, 2nd ed., McGraw-Hill, New York, 1968.
[8] R.P. Messmer, D.R. Salahub, K.H. Johnson, C.Y. Yang, Chem. Phys. Lett. 51 (1977) 84–89.
[9] W.A. Harrison, Pseudopotentials in the Theory of Metals, Benjamin, New York, 1966.
[10] M. Rasolt, R. Taylor, Phys. Rev. B 11 (1975) 2717–2725.
[11] P.C. Gehlen, J.R. Beeler, R.I. Jaffee, Interatomic Potentials and Simulation of Lattice Defects, Plenum, New York, 1971.
[12] M.I. Baskes, C.F. Melius, Phys. Rev. B 20 (1979) 3197–3204.
[13] M.S. Daw, M.I. Baskes, Phys. Rev. B 29 (1983) 6443–6453.
[14] M.S. Daw, M.I. Baskes, Phys. Rev. Lett. 50 (1983) 1285–1288.
[15] S.M. Foiles, M.S. Daw, W.D. Wilson, High Temperature Alloys: Theory and Design, The Metallurgical Society of AIME, New York, 1984.
[16] S.M. Foiles, Phys. Rev. B 32 (1985) 3409–3415.
[17] J.M.G. Miranda, V. Torra, J. Phys. F 13 (1982) 281–289.
[18] A. Maiti, L.M. Falicov, Phys. Rev. A 45 (1992) 6918–6921.
[19] E. Gregoryanz, O. Degtyareva, M. Somayazulu, R.J. Hemley, H.K. Mao, Phys. Rev. Lett. 94 (2005) 185502.
[20] L.A. Girifalco, V.G. Weizer, Phys. Rev. 114 (1959) 687–690.
[21] A.R. Ruffa, Phys. Rev. B 24 (1981) 6915–6925.
[22] J.K. Singh, J. Adhikari, S.K. Kwak, Fluid Phase Equilibr. 248 (2006) 1–6.
[23] D. Bhatt, A.W. Jasper, N.E. Schultz, J. Siepmann, D.G. Truhlar, J. Am. Chem. Soc. 128 (2006) 4224–4225.
[24] T. Aleksandrov, C. Desgranges, J. Delhommelle, Fluid Phase Equilibr. 287 (2010) 79–83.
[25] M. Canales, J.A. Padro, L.E. Gonzalez, A. Giro, J. Phys.: Condens. Matter 5 (1993) 3095–3102.
[26] M. Canales, L.E. Gonzalez, J.A. Padro, Phys. Rev. E 50 (1994) 3656–3669.
[27] R.W. Ohse, Handbook of Thermodynamics and Transport Properties of Alkali Metals, 1st ed., Blackwell, Oxford, 1985.
[28] N.T. Ban, C.M. Randall, D.J. Montgomery, Phys. Rev. 128 (1962) 6–11.
[29] D.K. Belashchenko, High Temp. 47 (2009) 494–507.
[30] D.K. Belashchenko, O.I. Ostrovski, High Temp. 47 (2009) 211–218.
[31] Y. Rosenfeld, Mol. Phys. 32 (1976) 963–977.
[32] Y. Rosenfeld, Phys. Rev. A 15 (1977) 2545–2549.
[33] Y. Rosenfeld, Chem. Phys. Lett. 48 (1977) 467–468.
[34] Y. Rosenfeld, J. Phys.: Condens. Matter 11 (1999) 5415–5427.
[35] H.J. Raveche, J. Chem. Phys. 35 (1971) 2242–2250.
[36] A. Baranyai, D.J. Evans, Phys. Rev. A 40 (1989) 3817–3825.
[37] M. Asta, D. Morgan, J.J. Hoyt, B. Sadigh, J.D. Althoff, D.d. Fontaine, S.M. Foiles, Phys. Rev. B 59 (1999) 14271–14281.
[38] S.M. Foiles, J.B. Adams, Phys. Rev. B 40 (1989) 5909–5915.
[39] J.J. Hoyt, M. Asta, B. Sadigh, Phys. Rev. Lett. 85 (2000) 594–597.
[40] M. Dzugutov, Nature 381 (1996) 137–139.
[41] S. Chapman, T.G. Cowling, The Mathematical Theory of Non-Uniform Gases, 3rd ed., Cambridge University Press, London, 1970.
[42] W.G. Hoover, Computational Statistical Mechanics, Elsevier, New York, 1991.
[43] G.X. Li, C.S. Liu, Z.G. Zhu, Phys. Rev. B 71 (2005) 094209.
[44] T. Goel, C.N. Patra, T. Mukherjee, C. Chakravarty, J. Chem. Phys. 129 (2008) 164904.
[45] J.D. Weeks, J. Chem. Phys. 67 (1977) 3106–3121.
[46] L. Vega, E.d. Miguel, L.F. Rull, G. Jackson, I.A. McLure, J. Chem. Phys. 96 (1992) 2296–2305.
[47] L.J.V. Poolen, C.D. Holcomb, V.G. Niesen, Fluid Phase Equilibr. 129 (1997) 105–111.
[48] M.P. Allen, D.J. Tildesley, Computer Simulation of Liquids, Oxford University Press, New York, 1987.
[49] J.K. Singh, J. Adhikari, S.K. Kwak, Mol. Phys. 105 (2007) 981–987.
[50] M. Matsumoto, Y. Takaoka, Y. Kataoka, J. Chem. Phys. 98 (1993) 1464–1472.
[51] S. Plimpton, J. Comput. Phys. 117 (1995) 1–19.
[52] F. Hensel, J. Phys.: Condens. Matter 2 (1990) SA33–SA45.
[53] A.W. Castleman, R.G. Keese, Science 241 (1988) 36–42.
[54] W. Freyland, Phys. Rev. B 20 (1979) 5104–5110.
[55] S.A. Rice, Mol. Simulat. 29 (2003) 593–609.
[56] J.S. Rowlinson, B. Widom, Molecular Theory of Capillarity, Clarendon Press, Oxford, 1982.
[57] R.M. Townsend, S.A. Rice, J. Chem. Phys. 94 (1991) 2207–2218.
[58] J. Gryko, S.A. Rice, J. Phys. F 12 (1982) L245–L250.
[59] J. Gryko, S.A. Rice, J. Non-Cryst. Solids 61–62 (1984) 703–706.
[60] R.W. Ohse, J.F. Babelot, J. Magill, M. Tetenbaum, Pure Appl. Chem. 57 (1985) 1407–1426.
[61] M.M. Martynyuk, Fazovye perekhody pri impul'snom nagreve (Phase Transitions under Pulsed Heating), Izd. RUDN (Russ. Univ. of Friendship of Peoples), Moscow, 1999.
[62] D. Bertolini, A. Tani, Phys. Rev. E 52 (1995) 1699–1710.
[63] B. Hong, F. Escobedo, A.Z. Panagiotopoulos, J. Chem. Eng. Data 55 (2010) 4273–4280.
[64] R.E. Meyer, N.H. Nachtrieb, J. Chem. Phys. 23 (1955) 1851–1854.
[65] A.V. Grosse, Science 147 (1965) 1438–1441.